Optimization of Lightweight and Misalignment Tolerance in Drone Wireless Charging Systems with Multi-parameter Optimization Designs

Yuhao Su

{su_yuhao@tju.edu.cn}

School of Chemical Engineering and Technology, Tianjin University, Haitang Street, Tianjin, China

Abstract. This paper investigates wireless charging systems for drones, focusing on key issues such as improving charging efficiency, enhancing misalignment tolerance, lightweight design, and multi-parameter optimization. First, the design and optimization of the resonant compensation network were conducted to improve the charging efficiency of the system. Second, the control system for wireless charging was optimized to enhance misalignment tolerance in complex charging environments. Finally, a multi-objective optimization of the magnetic coupling mechanism parameters in the wireless charging system was performed using the second-generation Non-dominated Sorting Genetic Algorithm (NSGA-II) and Latin Hypercube Sampling (LHS), aiming to enhance the system's overall lightweight and anti-misalignment performance. Experimental results show that the proposed optimization method significantly improves charging performance and provides an effective design strategy for parameter optimization in wireless drone charging systems.

Keywords: Drone, Wireless charging, Charging efficiency, Lightweight, Misalignment tolerance, Multi-objective optimization.

1 Introduction

1.1 Research Background

In recent years, with the rapid development of drone technology, drones have gained significant importance in areas such as agricultural monitoring, delivery services, and surveillance due to their simple structure, small size, low cost, and operational flexibility [1]. However, limited battery life remains a key challenge, restricting drone performance during extended tasks. To address this issue, wireless charging technology has emerged as a crucial solution to extend the operational time of drones. Wireless charging enables energy transfer from ground stations to aerial drones through electromagnetic induction or radiation, allowing for remote, contactless charging and increasing drone efficiency and operational duration.

Despite the promising potential of drone wireless charging technology, several challenges remain in practical applications. First, charging efficiency is a critical factor for system performance. Existing wireless charging systems present opportunities for improvement in the design of magnetic coupling mechanisms and circuit efficiency. Second, with the increasing diversity of drone application scenarios, lightweight design becomes essential. Reducing system

CONF-MLA 2024, November 21, Adana, Turkey

DOI 10.4108/eai.21-11-2024.2354615

weight without compromising charging performance is crucial for extending drone flight time and flexibility. Additionally, misalignment during flight due to drone movement can impact charging efficiency, necessitating enhanced misalignment tolerance in the system.

1.2 Literature Review

In the field of wireless charging technology, existing research has mainly focused on improving charging efficiency, enhancing misalignment tolerance, and lightweight design. Wei Xiaozhao [2] conducted an in-depth study on the LCC-LCC structure of wireless charging systems for electric vehicles and proposed methods to optimize the magnetic coupling mechanism and improve the compensation network to enhance overall system efficiency. Dai Womeng et al. [3] investigated the offset compensation method in LCC-S type wireless power transmission systems, demonstrating that this method can effectively enhance the system's misalignment tolerance, particularly in application scenarios with significant misalignment and load variations. Additionally, Jiang Jinhai [4] proposed a dynamic wireless power supply technology based on bipolar primary rails, which improves the stability of the system in complex environments by optimizing the coupling and transmission path, providing technical support for the dynamic adaptability of future wireless charging systems.

From the perspective of misalignment tolerance, Yan Hai et al. [5] proposed a magnetic resonant coupling wireless power transfer technology based on PP compensation structure. By optimizing the design of the magnetic coupling mechanism and compensation topology, this approach significantly improves system stability and efficiency, especially under various load conditions. Chen Deqing et al. [6] conducted a detailed analysis of energy losses in wireless charging systems and optimized magnet structures for different application scenarios, enabling the system to increase transmission efficiency while reducing energy losses, resulting in a more efficient wireless charging solution.

In summary, significant progress has been made in existing literature to improve the efficiency and stability of wireless charging systems. However, there is still substantial room for improvement in the field of multi-objective balanced optimization. Future research can build on current technologies, integrating advanced intelligent control strategies and optimization algorithms to achieve more efficient, stable, and adaptable wireless charging systems. This will not only meet the demands of existing applications but also provide more reliable technical support for emerging application scenarios, thereby promoting the widespread application of wireless charging technology across various fields.

This study focuses on addressing three key technological issues in drone wireless charging systems: improving charging efficiency, lightweight design, and enhancing misalignment tolerance. By tackling these challenges, this paper aims to improve the overall performance of drone wireless charging systems and provide efficient and reliable energy solutions for broader drone applications. Therefore, in-depth analysis and resolution of key issues in wireless charging systems, and improvement of wireless charging efficiency for drones, will be the key to promoting their widespread application in the industrial field.

2 Optimization of Charging Efficiency in Drone Wireless Charging Systems

2.1 Design and Optimization of Resonant Compensation Networks Wireless Charging System

Circuit Structure and Working Principle of Wireless Charging Systems. The circuit structure of a wireless charging system consists of several key components: a high-frequency inverter circuit, a magnetic coupling mechanism with a resonant compensation network, and a secondary energy conversion circuit [7]. The specific structure is shown in Figure 1.

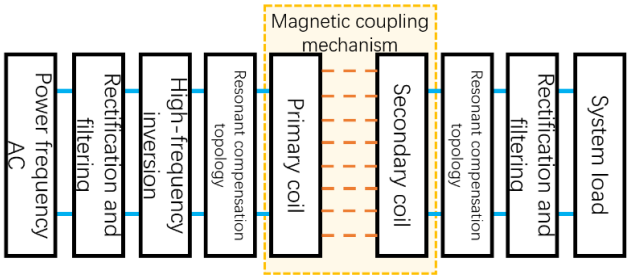

Fig. 1. Wireless Charging System Circuit Structure

(1) High-Frequency Inversion Section: Comprising rectification and high-frequency inversion, it converts AC mains power into DC and then into high-frequency AC through an inverter. This high-frequency AC drives the transmitting coil, generating a magnetic field for energy transmission.

(2) Resonant Compensation Network: By introducing specific inductances and capacitances at the transmitting and receiving ends, this network enables the system to achieve resonance at a certain frequency, reducing impedance and reactive power.

(3) Magnetic Coupling Mechanism: Consisting of transmitting and receiving coils, and their associated resonant compensation networks, the transmitting coil generates a high-frequency magnetic field that wirelessly transfers energy to the receiving coil.

(4) Secondary Energy Conversion Section: Converts the received high-frequency AC into stable DC power for use by the drone.

Analysis of Resonant Compensation Network Types. In wireless charging systems, variations in mutual inductance between the primary and secondary coils may occur due to distance and alignment issues. Resonant topologies use specific inductance and capacitance to maintain resonance, minimizing impedance and maximizing energy transfer efficiency at the resonant frequency.

Compensation networks are generally classified into S-S, S-P, P-P, and P-S types, where "S" refers to series and "P" to parallel configurations [8]. More complex hybrid compensation networks, such as LCC-LCC [2] and LCC-S [3], also exist. The P-P type network can achieve

efficient energy transfer, particularly under variable load conditions, and is relatively simple to design, making it suitable for lightweight, integrated drone systems. Therefore, this paper focuses on the design and control optimization of the P-P type compensation network.

2.2 Control Strategy for the P-P Resonant Compensation Network

Introduction. Drones typically use lithium batteries as energy storage devices. While the P-P network can theoretically provide constant current output, variations in load conditions and coil misalignment can disrupt the resonance state and output current [5]. To address this, suitable control strategies are needed to stabilize output current. Common control methods include frequency modulation, phase shift control, and DC-DC control [6]. Given the need for lightweight design, this study selects a DC-DC control system in the secondary circuit to adjust the output directly.

Principle and Modeling of Power Converters. The P-P network's high voltage gain requires the use of a Buck converter to step down voltage and achieve stable control. The Buck converter's PWM-controlled circuit is shown in Figure 2.

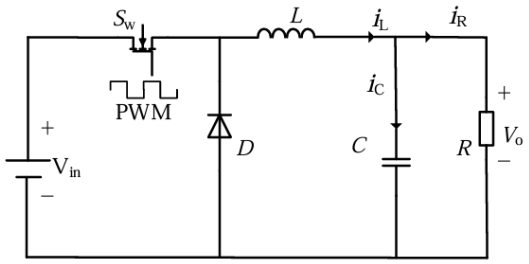

Fig. 2. PWM-Controlled Buck Circuit

In the Figure 2, Sw represents the power MOSFET, D is the freewheeling diode, and L and C represent the energy storage inductor and filter capacitor, respectively. By switching Sw, input voltage is converted into a rectangular waveform, and the LC filter extracts a stable DC voltage output (Vo). The average state equation for the system in one period (T) is given by the following equations:

$$\begin{cases} \mathrm{L}\dfrac{\mathrm{d}\left(\mathrm{i}(\mathrm{t})+\mathrm{i}(\mathrm{t})\right)}{\mathrm{dt}} = \left(\mathrm{D}+\hat{\mathrm{d}}\right)\mathrm{v}_{\mathrm{in}}(\mathrm{t}) - \left(\mathrm{v}_{\mathrm{o}}(\mathrm{t})+\hat{\mathrm{v}}_{\mathrm{o}}(\mathrm{t})\right) \\ \mathrm{C}\dfrac{\mathrm{d}\left(\mathrm{v}_{\mathrm{o}}(\mathrm{t})+\hat{\mathrm{v}}_{\mathrm{o}}(\mathrm{t})\right)}{\mathrm{dt}} = \left(\mathrm{i}(\mathrm{t})+\hat{\mathrm{i}}(\mathrm{t})\right) - \dfrac{\left(\mathrm{v}_{\mathrm{o}}(\mathrm{t})+\hat{\mathrm{v}}_{\mathrm{o}}(\mathrm{t})\right)}{\mathrm{R}} \end{cases} \tag{1}$$

where D is the duty cycle of the PWM control signal.

The transfer function of the Buck converter, including inductance current and output voltage:

$$G_{id}(s) = \frac{\hat{i}(s)}{\hat{d}} = \frac{V_{in}(Cs+1/R)}{LCs^2+L/R^{s+1}} \tag{2}$$

$$G_{\mathrm{vd}}(s)=\frac{\hat{v}_{\mathrm{o}}(s)}{\hat{d}}=\frac{V_{\mathrm{in}}}{LCs^{2}+L/R^{s+1}} \tag{3}$$

Control Strategy for Power Converters. Buck converters are typically controlled using one of three methods: Pulse Frequency Modulation (PFM), Pulse Width Modulation (PWM), or PWM/PFM hybrid control. This study selects the PWM method, and within PWM, three sub-methods are considered[4]:

(1) Voltage Mode Control

(2) Peak Current Mode Control

(3) Average Current Mode Control

Among these, average current control provides faster transient response and higher stability, with simpler circuitry and automatic current-sharing capabilities, making it the most suitable for this study.

Converter Design Based on Average Current Mode Control. In the previous section, the selection of the converter and the control strategy was preliminarily determined, with the choice to use average current control. To achieve control of both current and voltage, average current control includes two closed-loop control loops: the inner loop compensates for current, while the outer loop compensates for voltage.

For the current inner loop compensation, according to equation (4), the transfer function of the inductor current is obtained:

$$G_{\mathrm{id}}(s)=\frac{\hat{i}(s)}{\hat{d}}=\frac{V_{\mathrm{in}}\left(Cs+\frac{1}{R}\right)}{LCs^{2}+\frac{L}{R}s+1} \tag{4}$$

The PI compensator controls the current inner loop, and its compensation function is:

$$G_{\mathrm{i}}(s)=K_{\mathrm{ip}}+\frac{K_{\mathrm{ii}}}{s} \tag{5}$$

To ensure system stability, the phase margin after compensation is set to 60°, and the following equation is derived:

$$\begin{cases} |G_{\mathrm{i}}(s)\cdot G_{\mathrm{id}}(s)|_{s=j\omega_c}=1 \\ \angle G_{\mathrm{i}}(s)\cdot G_{\mathrm{id}}(s)|_{s=j\omega_c}=-\dfrac{2\pi}{3} \end{cases} \tag{6}$$

ω_c—crossover frequency (in PI control, the crossover frequency is generally selected as 1/10 to 1/5 of the switching frequency). By solving, we get:

$$\begin{cases} K_{\mathrm{ip}} \\ K_{\mathrm{ii}} \end{cases} \tag{7}$$

Based on the following experimental parameters, the Bode plots can be obtained:

$V_{in} = 35V$, $V_o = 16V$, $L = 40\mu H$, $I_o = 16V$, $C = 100nF$, $f_s = 140kHz$, $R = 7.5\Omega$, $\omega_c = f_s/10$

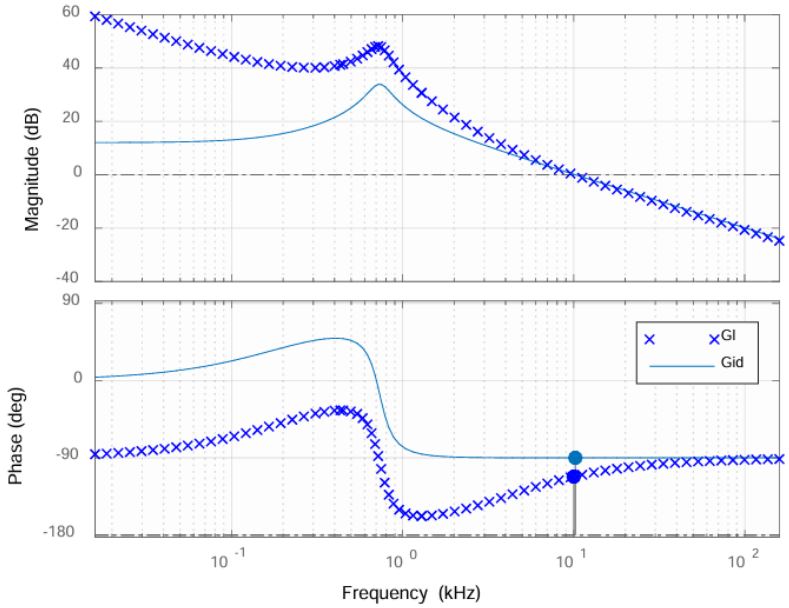

Fig. 3. Bode Plot of Current Inner Loop Before and After Compensation

By calculating $G_1 = G_i(s) \cdot G_{id}(s)$,and comparing the Bode plots before and after compensation, the compensation effect of the inner loop compensation circuit can be evaluated.

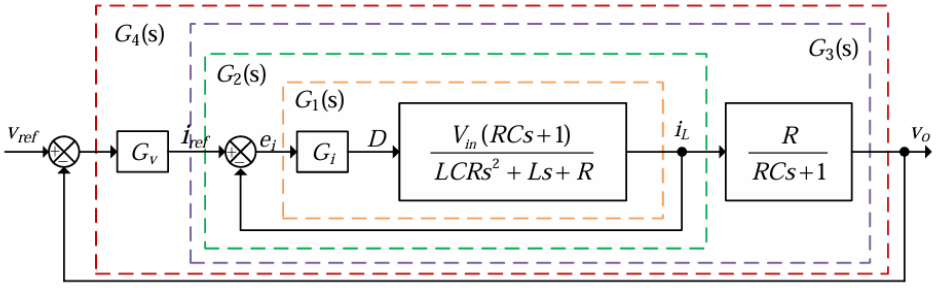

Fig. 4. Double Closed-loop PI Control Block Diagram

For the voltage outer loop compensation, based on the previous discussion, the compensated transfer function of $i_L(s)$ with respect to $e_i(s)$ is $G_1(s)$:

$$G_1(s) = G_i(s) \cdot G_{id}(s) = \frac{K_{ip}s + K_{ii}}{s} \cdot \frac{V_{in}(Cs + 1/R)}{LCs^2 + L/R^{s+1}} \tag{8}$$

The compensated transfer function of $i_L(s)$ with respect to $i_{ref}(s)$ is $G_2(s)$:

$$G_2(s) = \frac{G_1(s)}{1 + G_1(s)} = \frac{RCK_{ip}V_{in}s^2 + (K_{ip} + RCK_{ii})V_{in}s + K_{ii}V_{in}}{LRCs^3 + (L + RCK_{ip}V_{in})s^2 + (R + K_{ip}V_{in} + RCK_{ii}V_{in})s + K_{ii}V_{in}} \quad (9)$$

The compensated transfer function of $v_o(s)$ with respect to $i_{ref}(s)$ is $G_3(s)$:

$$\begin{aligned} G_3(s) &= G_2(s)\frac{R}{1 + RCs} \\ &= \frac{RK_{ip}V_{in}s + RK_{ii}V_{in}}{LRCs^3 + (L + RCK_{ip}V_{in})s^2 + (R + K_{ip}V_{in} + RCK_{ii}V_{in})s + K_{ii}V_{in}} \end{aligned} \quad (10)$$

After PI compensation, the compensation function of the outer loop voltage is:

$$G_v(s) = K_{vp} + K_{vi}/s \quad (11)$$

The open-loop transfer function is:

$$G_4(s) = G_v(s) \cdot G_3(s) = \frac{K_{vp}s + K_{vi}}{s} \cdot \frac{R}{1 + RCs} \cdot \frac{G_i(s) \cdot G_{id}(s)}{1 + G_i(s) \cdot G_{id}(s)} \quad (12)$$

To ensure system stability, the phase margin after compensation is set to 60°, and the following equation is obtained:

$$\begin{cases} |G_4(s)|_{s=jw_c} = 1 \\ |G_4(s)|_{s=jw_c} = -\pi/2 \end{cases} \quad (13)$$

By solving equations (12), (13), and (14) simultaneously, we get:

$$\begin{cases} K_{vp} \\ K_{vi} \end{cases} \quad (14)$$

Using the same parameters, the following Bode plots can be obtained.

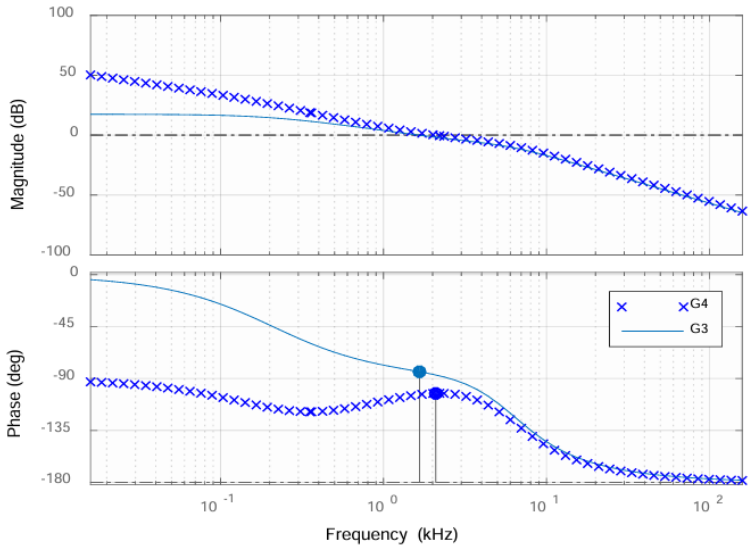

Fig. 5. Bode Plot of Voltage Outer Loop Before and After Compensation

By comparing the Bode plots of the open-loop transfer functions $G_3(s)$ and $G_4(s)$ before and after compensation, the compensation effect of the inner loop compensation circuit can be evaluated.

By integrating the above two compensation circuits, the rationality of the inner and outer loop compensator design can be verified based on the selected converter parameters.

3 Multi-parameter Optimization of the Drone Wireless Charging System

3.1 Drone Parameter Optimization Problem

Overview of Multi-objective Optimization. In the optimization process of wireless charging systems, there are various evaluation criteria, such as efficiency, output power, the mutual inductance range of the magnetic coupling mechanism, and weight. Optimizing one parameter may affect the performance of others, for example, increasing output power may lead to a higher weight. Therefore, it is not advisable to optimize just a single criterion.

To address this issue, multi-objective optimization algorithms can be employed. Unlike single-objective optimization, which typically results in a single solution, multi-objective optimization provides a set of solutions. These solutions are known as Pareto optimal solutions, and the set they form is called the Pareto front (PF). However, solutions in the Pareto front cannot be simply compared by a superior-inferior relationship. The core goal of multi-objective optimization is to find the Pareto optimal solution set to achieve parameter optimization.

Evaluation Criteria for Multi-objective Optimization Algorithms. Before discussing the evaluation criteria, it's important to understand the following terms [9]:

1. Pareto Dominance:

In multi-objective optimization, if one solution performs better than another on all objectives, it is said to "dominate" the other solution.

2. Pareto Optimal Solution:

A Pareto optimal solution is one that is not dominated by any other solution. This means that no other solution can improve one objective without worsening at least one other objective. In other words, a Pareto optimal solution represents the best trade-offs among multiple objectives.

3. Pareto Optimal Solution Set:

This is the collection of all Pareto optimal solutions, and none of them dominates another. Each solution represents the best balance for different objectives.

4. Pareto Front:

The Pareto optimal solution set mapped to the objective space forms the boundary called the Pareto front, which typically represents the limit of all "best" solutions in a multi-objective optimization scenario.

The core goal of multi-objective optimization algorithms is to find the Pareto optimal solution set and the Pareto front. The evaluation of multi-objective optimization results typically includes

two aspects: how close the solution set is to the Pareto front and whether the individuals in the set are evenly distributed. This paper adopts the Inverted Generational Distance (IGD) as an evaluation metric [10], which calculates the average shortest distance between each solution and a reference set uniformly distributed on the Pareto front. A smaller average value indicates better convergence and distribution, as shown in equation (15):

$$IGD = \frac{\sum_{i=1}^{N} min\left(d(v, PF^*)\right)}{N} \tag{15}$$

Where N is the number of individuals in the Pareto solution set found by the algorithm, v is an individual, PF^* is an individual in the reference set, and d is the Euclidean distance between them.

3.2 Selection of Multi-objective Algorithms

The CEC test set is commonly used to evaluate and compare the performance of different optimization algorithms, especially in multi-objective and global optimization problems. This paper uses test functions from the CEC2021 test set, selecting seven functions. The goal of optimization for all functions is to minimize the value of each sub-function, and their Pareto fronts exhibit different characteristics (e.g. ZDT2, ZDT6, Kita, and DTLZ functions have convex Pareto fronts; ZDT1, ZDT4 have non-convex fronts, and the ZDT3 front is a discontinuous line segment). The ZDT5 function, which uses binary coding and has limited variable ranges, is excluded. Each algorithm performs 50 repeated experiments on each function, comparing the best, worst, and average IGD. The smaller the IGD, the stronger the optimization capability of the algorithm.

Table 1. Numerical Experiment Results of Various Multi-Objective Optimization Algorithms

		F1	F2	F3	F4	F5	F6	F7
NSGA-II[11]	BEST	0.82633	0.65612	1.268859	0.73046	0.55585	0.54255	0.750704
	WORST	1.84847	1.96987	11.84169	12.43558	3.135424	1.16033	1.614683
	AVG	1.12385	1.11268	2.961836	1.30637	0.77952	0.80898	1.070159
MOPSO [12]	BEST	1.234886	1.099569	1.31795	1.20977	1.125339	0.809491	0.70235
	WORST	2.270709	1.881339	4.28946	2.532768	2.41219	1.436588	1.31522
	AVG	1.502437	1.378716	1.77601	1.525051	1.500034	1.11185	1.0583
BPSO1 [13]	BEST	30.62874	24.06794	22.89918	6.355248	56.59997	7.414222	4.58184
	WORST	647.7584	942.3512	980.0889	168.7672	63.77148	163.0044	79.08461
	AVG	87.78781	287.1787	641.2318	69.34512	60.25904	67.37144	74.05153
BPSO2	BEST	34.51287	34.62691	18.76288	4.282093	55.47379	14.92747	2.154516
	WORST	962.1836	942.3512	980.5302	63.89543	64.27901	163.0044	78.26657
	AVG	289.1266	476.7457	738.1243	17.26492	59.50034	84.67858	55.20632

DE1[14]	BEST	63.90577	69.17557	109.9627	67.28569	55.82224	50.15055	72.6971
	WORST	73.61178	78.54924	119.5418	74.56483	64.37751	60.57395	77.6658
	AVG	69.54472	74.21825	114.5514	71.11977	60.03732	56.24749	75.35775
DE2	BEST	37.19271	68.63122	110.6084	34.44157	54.64699	52.64059	38.31232
	WORST	38.00001	78.47911	118.4664	42.32861	64.96864	62.47802	43.23736
	AVG	37.90596	73.14763	114.7791	38.16626	60.13326	57.2761	40.71459

The results show that NSGA-II performs best in terms of average optimization capability for ZDT1, ZDT2, ZDT4, ZDT6, and Kita functions. Therefore, NSGA-II is selected as the multi-parameter optimization algorithm for the drone.

4 Parameter Optimization of Lightweight Magnetic Coupling Mechanism Based on NSGA-II

4.1 NSGA-II and Latin Hypercube Sampling (LHS)

NSGA-II Algorithm. The Genetic Algorithm (GA) is an evolutionary algorithm that simulates the natural selection process, where individuals that better adapt to their environment are selected, and their offspring inherit genes while undergoing crossover and mutation. Through generations of selection, the optimal solution is obtained. The second-generation Non-dominated Sorting Genetic Algorithm (NSGA-II) is an improvement of GA that introduces the concept of dominance and uses dominance relationships to determine the quality of individuals[15]. Dominant individuals are more likely to pass on their traits. NSGA-II also introduces a crowding strategy, which refers to the largest rectangular space between one individual and others. Higher crowding indicates greater individual diversity. This strategy ensures the diversity of solutions.

Latin Hypercube Sampling (LHS). At the start of the genetic process, an initial population is needed. In random sampling, parameter values are selected arbitrarily, which may lead to dense sampling in some areas and sparse sampling in others. LHS divides each parameter range into multiple equal intervals, ensuring that each interval contains at least one sample point. LHS ensures uniform distribution of sampling points across dimensions, enhancing the diversity of parameter combinations.

4.2 Parameter Optimization Method for Lightweight Magnetic Coupling Mechanisms

Parameter Selection. The racetrack-shaped coil coupling mechanism consists of a racetrack transmitter and a square receiver. Due to its large mutual inductance and strong anti-misalignment capability, it is often used in wireless power transfer systems. The key parameters include inner coil size Ln, the number of turns for the inner and outer layers of the transmitter N1, N2, receiver turns NR, and transmission distance H. When evaluating the anti-misalignment capability, the radius of the incircle R, which forms the boundary where the mutual inductance drops to 50% of its aligned value, is used as the evaluation metric. Therefore, R is set as the optimization target. To balance lightweight design and anti-misalignment performance, smaller Ln and NR, and larger R and H are required.

Optimization Process. First, constraints are imposed on the parameters Ln (55-95mm), N1 (1-20), N2 (1-20), NR (1-20), and H (50-150mm) and Latin Hypercube Sampling is used to generate the initial population within these constraints. Then, each individual in the population undergoes simulation analysis to obtain R and calculate fitness. Fast non-dominated sorting is performed, and if convergence conditions are not met, the individuals are selected, and crossover and mutation are applied to generate offspring. The offspring and parents are combined, and the process is repeated. After multiple cycles, the proportion of first-level individuals—those with the strongest dominance—stabilizes. The solution set formed by these individuals is mapped into space, producing the Pareto front. Solutions at the extremes of the Pareto front, which perform well in some parameters but poorly in others, should be discarded to ensure a comprehensive balance of parameter performance.

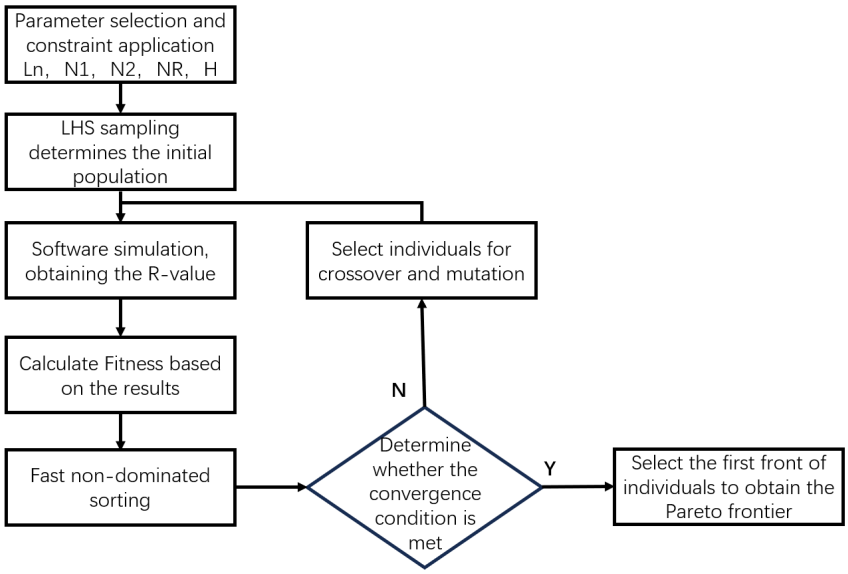

Fig. 6. optimization flowchart.

After the algorithm converges, the individuals at both ends of the Pareto front in the first layer are discarded, followed by further screening. Finally, the transmission distance of 50 mm is

selected, with the inner coil size of 65 mm, and the number of turns for the outer and inner coils being 19 and 10, respectively, while the receiving end has 18 turns. The relationship between the total mutual inductance and the offset distance is shown in the figure, where it can be observed that these parameters improve the anti-offset capability within a certain range of conditions.

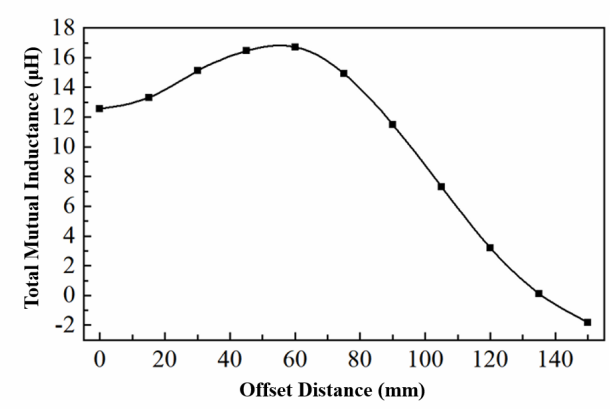

Fig. 7. Graph of Total Mutual Inductance vs. Offset Distance

The NSGA-II algorithm not only balances anti-misalignment capability and lightweight design but can also be applied to parameter optimization in other areas, such as compensation network parameters, making NSGA-II an effective optimization method in future research.

5 Conclusion

This paper addresses key issues in drone wireless charging technology, proposing several solutions and conducting in-depth analysis and optimization. Regarding charging efficiency, the resonance compensation network was optimized to improve energy transmission efficiency. For anti-misalignment capability, the coupling mechanism and compensation topology were optimized, enhancing system stability. Moreover, multi-objective optimization algorithms were used to achieve a balanced improvement in all performance metrics of the drone wireless charging system. With further technological advancements, drone wireless charging systems will have broader applications, providing more reliable energy support for long-term, stable drone operations.

References

[1] Wu, Shuai, Cai, Chunwei, Chen, Yi, et al. Research Progress and Development Trends of Wireless Charging Technology for Multi-Rotor Drones. Journal of Electrical Engineering, 2022, 37(03): 555-565.

[2] Wei Xiaozhao. Research on Several Issues of Wireless Charging for Electric Vehicles with LCC-LCC Structure [D]. Shandong University, 2021.

[3] Dai Womeng, Li Zhizhong, Zhang Haonan, Li Jiefan. Offset Compensation Method Based on LCC-S Type WPT System [J]. Power Electronics Technology, 2023, 57 (08): 82-85.
[4] Jiang Jinhai. Research on Dynamic Wireless Power Supply Technology Using Bipolar Primary Rails [D]. Harbin Institute of Technology, 2019.
[5] Yan Hai, Mao Xingkui, Zhou Zhiwei. Research on Magnetic Resonant Coupling Wireless Power Transfer Technology Based on PP Compensation Structure [J]. Electrical Appliances and Energy Efficiency Management Technology, 2019, (17): 15-20.
[6] Chen Deqing, Wang Lifang, Liao Chenglin. Loss Analysis and Magnet Structure Optimization of Wireless Charging Systems [J]. Transactions of China Electrotechnical Society, 2015, 1(9): 2-5.
[7] Zhang, Peng. Design of a High Power Density Modular Wireless Charging System for Drones. Harbin Institute of Technology, 2021.
[8] Sun Xuege. Analysis and Design of a Strong Misalignment Tolerance and Lightweight Coupling Mechanism for UAV Wireless Charging Systems [D]. Chongqing University, 2021.
[9] Liu Wei, Zheng Huanqi, Zhou Yucheng. Research on Multi-Objective Optimization Control Strategy for Fresh Air Systems Based on Improved NSGA-II [J]. Modern Electronics Technique, 2024, 47 (15): 169-177.
[10] Liu, Hao. Research on the Performance Improvement of Magnetic Coupling Mechanism in Wireless Charging Systems for Rotor Drones. Northeast Forestry University, 2023.
[11] Jia Huihui. Research on Software Test Case Selection Based on Improved NSGA2 Algorithm [D]. Anhui University, 2023.
[12] Yang Wen, Ye Shuai, Yao Qishui, Yu Jianghong, Hu Meijuan. High-Speed Ball Bearing Optimization Design Method Based on Multi-Objective Particle Swarm-Genetic Hybrid Algorithm [J]. Electromechanical Engineering, 1-11.
[13] Chen Jian, Huang Zhi, Xu Tingliang, Sun Taihua, Li Xueyuan. Bearing Fault Diagnosis Based on Improved Binary Particle Swarm Algorithm Optimized DBN [J]. Modular Machine Tool & Automatic Manufacturing Technique, 2024, (01): 168-173.
[14] Zhou Li, He Rongyu, Li Hao, Tang Hui, Yang Liuxiangzi, Xia Yule. Design of Robotic Arm Trajectory Planning Based on Improved DE Algorithm [J]. Automation Technology and Applications, 2024, 43 (09): 12-15+41.
[15] Ma, Shuo. Research on Multi-Objective Vehicle Routing Problem Based on Non-Dominated Sorting Genetic Algorithm. Dalian Maritime University, 2019.